**CERN-ACC-2014-0244**

2014-10-30

Mikko.Karppinen@cern.ch

# New Mechanical Concept for Nb3Sn Quadrupole

*M. Karppinen*
CERN TE-Department, Geneva, Switzerland

**Keywords:** LHC, HL-LHC, HiLumi LHC, High-field magnet, Quadrupole, $Nb_3Sn$

**Abstract**

A new mechanical design concept for the Nb3Sn quadrupoles has been developed with a goal of an accelerator quality magnet that can be industrially produced in large series. This concept can easily be extended to any length and applied on both 1-in-1 and 2-in-1 configurations. It is based on the pole-loading concept and collared coils using dipole-type collars. First conceptual design study using finite element analysis has been carried out using the present base-line HL-LHC IR quadrupole QXF coil geometry for direct comparison with the bladder-and-key structure. The main features of the new design concept are described and the main results of the structural analysis discussed.

# Contents

# 1 Introduction

The future upgrades of the CERN accelerator chain along with the future high-energy colliders, notably the FCC, will require high gradient quadrupoles. The most likely option for the conductor technology today is the Nb3Sn, which sets stringent requirements for the coil fabrication technology and the mechanical structure of the magnet cold mass. Any larger series of magnets shall be industrially produced whilst respecting the criteria of accelerator quality magnets in terms of the magnetic performance, reproducibility, and reliability. Given the significant investment in conductor, the losses during the manufacturing process shall be minimized by careful engineering of the magnet cold mass and the optimisation of the production tools and procedures.

At CERN a long experience from industrially produced accelerator magnets has been acquired over the years culminating in the successful series production of the LHC Main Dipoles (MB) and Main Quadrupoles (MQ) along with special magnets for the insertion regions. They all share similar well-proven features like collared coils and laminated iron yokes for clamping the Nb-Ti coils under the influence of very high electro-magnetic forces. The manufacturing methods have been well optimised over the years and significant production infrastructure exists and is fully operational at CERN for various magnet types and lengths up to 15 m. The collar and yoke laminations are typically fine-blanked with very tight tolerances at the 20 µm level, which enables very good reproducibility and manufacturing accuracy for long magnets and series production.

As part of the HL-LHC project, the 11 T Dipole is the first Nb3Sn magnet designed from the beginning to be compatible with the accelerator requirements and industrial production [1]. Several new features are now being qualified through 11 T dipole short model program and work on the scale-up to a full-size prototype magnet of 5.5 m is underway. The mechanical concept, based on the pole-loading principle, has been further developed for a Nb3Sn quadrupole using dipole-type collars. This report describes this new concept and gives the results of the initial design optimisation using a fully parametric finite element model. For benchmarking purposes and to compare with the present base-line design of the HL-LHC IR quadrupole QXF, based on bladder-and-key concept, this initial conceptual study is made with identical coils and quasi-identical magnetic characteristics. Such design featuring 140 T/m gradient in 150 mm coil aperture is significantly more demanding mechanically than the present FCC IR Quadrupole parameters (200 T/m, 90 mm aperture) [2] and, as such, provides the FCC optics studies an idea of the upper limit of such magnet with presently available technology. This new concept can also be easily extended for the 2-in-1 configuration that will be required for the FCC main quadrupoles.

# 2 Mechanical concept

## 2.1 Common concepts used in present Nb3Sn accelerator magnet programs

The Nb3Sn coil technology developed in the frame of the US-LARP program [3] is based on the poles, typically made of Ti-alloy, being integrated in the coils during the vacuum impregnation with epoxy-resin. This limits possible adjustment of the coils size in the case of dimensional deviations from the nominal coil geometry. In addition, the tuning of the coil pre-compression by shimming is limited to coil mid-plane and the radial interface between the coil and the surrounding structure. The collared structure used in “traditional” Nb-Ti accelerator magnets generally relies on the pole shim in the tuning of the pre-stress and also for the correction of the field harmonics.

The Nb3Sn quadrupoles and dipoles developed at FNAL [4] based on collared coils are pre-loaded by introducing elliptic deformation at the coil mid-planes to bring the pole pre-stress to the required level without over-loading the mid-plane turns. Bending the coils requires careful monitoring

of the coil stress with strain gauges during the magnet assembly. The available locations for strain gauges mounted on substrate with known mechanical properties are very limited and for practical reasons the instrumentation can only be applied on the inner surface of the coil. The interpretation of the strain gauge signals on coils pre-loaded by bending requires knowledge of the neutral axis making this analysis very challenging with relatively large error bars.

Quadrupole-type collars made of four sectors were used in the FNAL TQC model magnets [5]. This type of collars has been widely used in Nb-Ti quadrupoles, but is not well suited for Nb3Sn quadrupoles, because the collars have to be pushed in incrementally over the magnet length causing unavoidable local shear stress in the fragile coils. Due to the delicate nature of this operation the assembly time is very long making it less suitable for series production.

The bladder-and-key concept [6] developed at LBNL provides an interesting alternative to the collared coil structure. The coil pre-compression is based on tuning the radial pressure from the surrounding structure. During the assembly the stainless steel bladders filled with pressurised water are used to create the radial pressure on the coils and, once the desired level of pressure is reached, the bladders are replaced by keys. This concept is very well suited for model magnets, as the assembly parameters can relatively easily be modified by altering the key dimensions. It, however, heavily relies on the strain gauges, which in general have limited reliability when applied on the Nb3Sn coils and usually an indirect signal from gauges mounted the Al-outer shell is used for this purpose. The other limitation is the maximum bladder pressure of about 55 MPa, which means that this concept relies on differential thermal contraction to bring the coil pre-stress to the required level during the cool down. With this the cold mass is not static with a dimensionally well-defined configuration, but instead there is a dynamic balance between the coils reacting against the outer shrinking cylinder. This concept also requires an additional stainless steel shell welded around the Al-shell for the He-containment of the cold mass. The scale-up for longer magnets addressing all requirements for accelerator magnets (alignment, reproducibility, field quality, etc.) has yet to be demonstrated and the first results in this sense are expected in 2016-17 [7].

### 2.1 Pole loading concept

To address the above-mentioned limitations and to make use of the extensive experience of collared coils a new concept for Nb3Sn dipole was developed and implemented in the CERN 11 T Dipole model magnets. The main difference from the US coil concept is that the Ti-alloy pole is not part of the coil, but inserted during the assembly process. This allows shimming at the pole and uses the collars more efficiently for creating the coil pre-stress, similarly to the collared Nb-Ti accelerator magnets and not relying on elliptic deformation of the coils.

The first 11 T Dipole practise model [8] in single coil configuration was recently tested and demonstrated very good training performance validating this concept. The first full single-aperture model test is expected in October this year.

The concept has now been further developed for a quadrupole. The pole region of the coils is identical to the dipole and the collared coil is based on dipole-type collars. This has some implications on the design of the pole area at the mid-plane of the top and bottom collars. The main advantages of this are that the collaring is done simultaneously over the entire coil length thus avoiding local shear stress in the coil, and the use of existing infrastructure (collaring presses) and well-known assembly procedures. The dipole-type collaring of quadrupole coils was already chosen as the base-line for SSC QSE magnets [9] and FNAL successfully re-assembled and tested a set of TQ-coils [10] using dipole-type collars. It should be noted, however, that the TQ-coils had integrated poles and the coils had already been through several assembly iterations in a bladder-and-key structure.

### *2.1.1 Coil design*

The coil fabrication process of the pole-loading concept is identical to the coils developed at FNAL except for the pole region. The pole angle of the inner and outer winding layers is aligned by inserting additional filler wedge on the outer layer as illustrated in Figure 1. A separate reaction pole is used during the reaction and then removed when the coil is prepared for the impregnation. To protect the coil and to distribute the pole pressure more evenly across the coil 2-mm-thick stainless steel loading plates are added at the pole and a separate impregnation pole provides accurate size for the pole region of the impregnated coil.

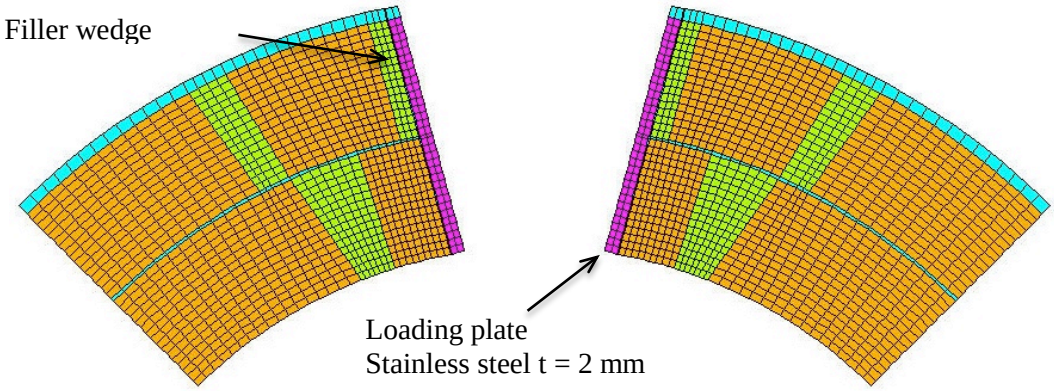


Figure 1 QXF coil FE-model adapted for pole-loading concept.

In the coil ends the first end spacer, which is the extension of the pole, has a slot as shown in Figure 2. The "legs" of this spacer align with the loading plates of the straight section. A short pole wedge of 150 mm is used across this transition from straight to the end region. The pole adjustment shim shown between the collar and this short wedge is reduced by 0.2 mm such that towards the end the short pole wedge section sits radially 0.2 mm further out thus reducing linearly the coil stress. This is to avoid discontinuous stress pattern in this delicate area minimising any shear stress in the reacted Nb3Sn coils. The first end spacer has an longitudinal slit to make it more flexible. The other end spacers feature similar swivel joints in the spacer "legs" to 11 T dipole spacers to minimise the risk of insulation damage during the fabrication process. The end spacers can be made of stainless steel by selective laser-sintering (SLS) and after reaction the end saddles can be replaced by G11 parts to better match the rigidity of the end region with the straight section and to make the electrical insulation of the splice region more robust.

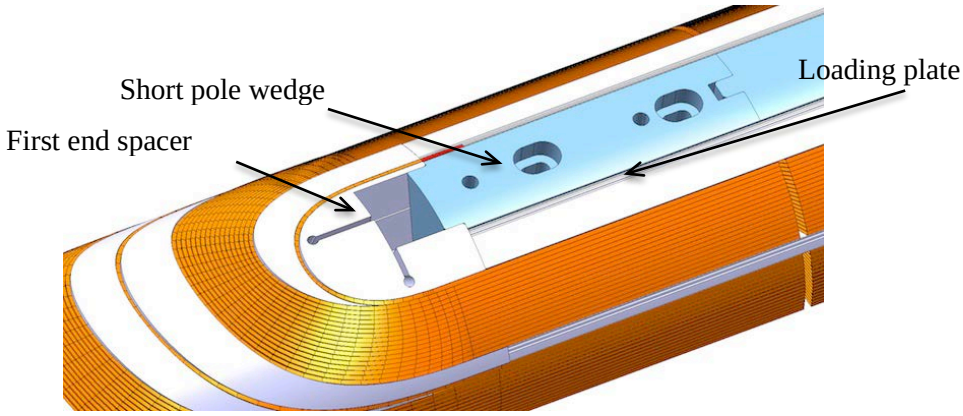


Figure 2 11 T Dipole coil return end showing the transition between coil straight section and the end region.

### *2.1.2 Collared coil*

The four coils are assembled together with the appropriate ground insulation that goes around the coil mid-plane and over the loading plate at the pole. The pole wedges are then inserted in the coils, which

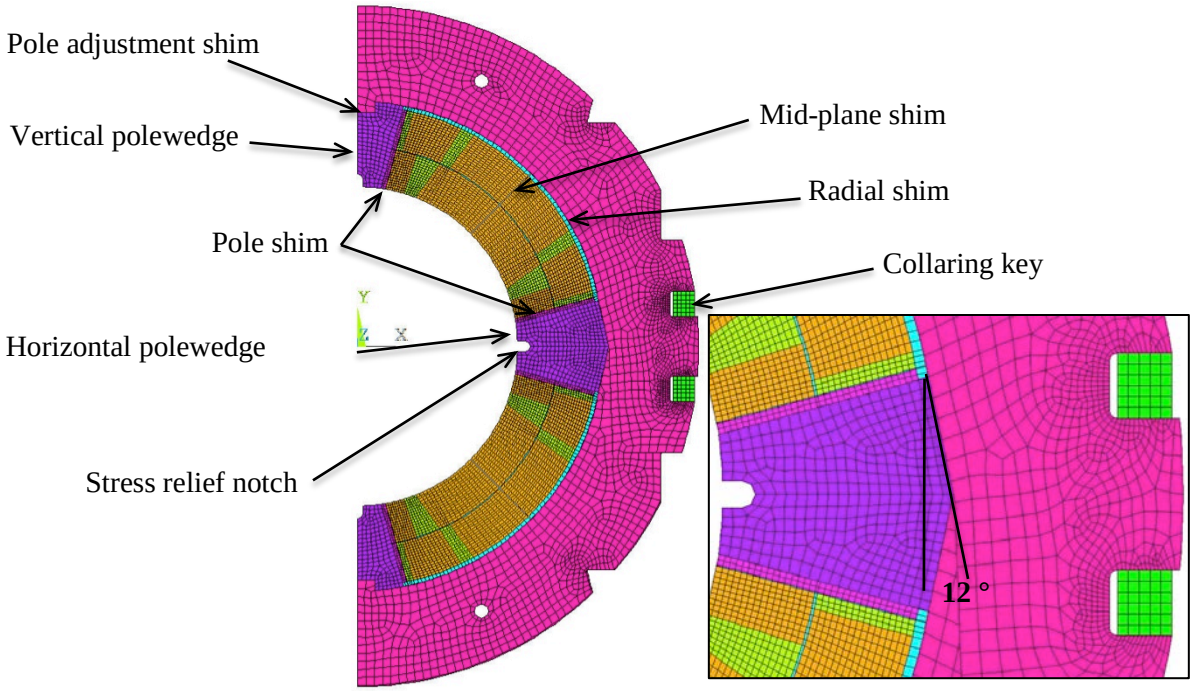


Figure 3 Collared coil main components and shim locations.

also secures the ground insulation in place. The pole wedges in the vertical axis in Figure 3 are similar to the 11 T Dipole pole wedges with the alignment slot that locates the collar nose and transmits the vertical force from the collars to the pole wedge.

In the mid-plane the pole wedge has a 12° taper such that the long collars with similar taper near the mid-plane push the wedge radially in during the collaring. With the present dimension the radial stroke is about 1.2 mm. This pole wedge is dimensioned such that its radial position is identical to the pole wedge at the vertical plane after collaring when the load is taken by the collaring keys.

The locations of adjustment shims are also shown in Figure 3. The pole and mid-plane shims are primarily used for adjusting the pre-stress and the radial shim between the collar and the coils can be used to compensate the dimensional differences of the coils. In addition, the shim between the pole wedge and the collar can be used at the model phase to adjust the pre-loading by adjusting the radial position of the wedge relative to the coil without taking the coil assembly apart. These shims would not be used once a good dimensional reproducibility of the coils has been reached.

### *2.1.3 Yoke and shell*

The laminated iron yoke is made in two halves and, depending on the deformation of the collared coil, either horizontal or vertical split can be used. The yoke inner diameter has line-to-line fit with the nominal collar outer contour. There is a shim between the collared coil and the yoke that allows positive and negative adjustment of this interface. The contact area can also be limited to cover only part of the circumference, if necessary. Figure 4 illustrates the cold mass cross-section.

Compared to the collared coil, the yoke halves can be considered almost infinitely rigid. It is, therefore, possible to bring an ovalised collared coil back to the circular shape in the yoking press. The ideal solution is to close the yoke gap during the yoke assembly and keep it closed at all times. This

creates an extremely rigid structure to sustain the magnetic forces and to avoid coil deformation that can have a deleterious effect on quench performance and field quality.

The differential thermal contraction of the yoke and the collared coil shall, however, be accounted for such that contact in this interface is preserved at the operating temperature. This, in turn, may require the yoke gap to remain slightly open at ambient temperature and then close during the

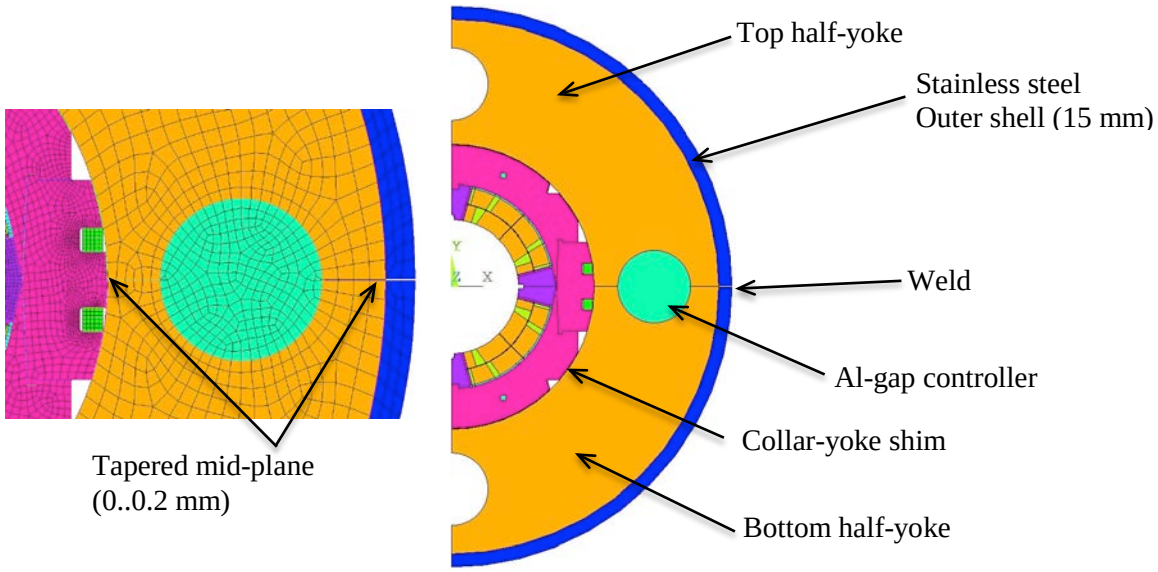


Figure 4 Magnet cross-section with main cold mass components.

cool down. An open gap is very difficult to accurately control during the yoke assembly in the powerful welding press and it is better to press against a known reference plane (displacement control instead of force/pressure control). In single aperture quadrupoles operating at superfluid helium one or two heat exchanger tubes typically run though the yoke. For symmetry reason additional two holes are added in the yoke laminations and can be used for mechanical purposes. Al-bars or thick-walled tubes inserted in the mid-plane holes act as gap controller allowing an accurate adjustment of the yoke gap during the assembly phase. By appropriate dimensioning, the differential thermal contraction results in the closure of the yoke gap during the cool down whilst preserving a static and very rigid structure around the coil at all times.

The stainless steel outer shell is made in two halves and welded around the yoke in the welding press. Weld shrinkage of up to 1 mm can be obtained with present welding techniques and typically the shell tension is kept below 200 MPa at the ambient temperature.

## 3 Structural analysis

The present base-line design for the HL-LHC IR-quadrupole, QXF, which has been extensively optimised over the past few years, has been taken as a reference for this initial conceptual study. For this reason the coils used in the structural analysis are identical to those used in the FEA of the QXF [11]. The large aperture of 150 mm and 140 T/m nominal gradient represent a significant challenge for the mechanical structure and hence a very good benchmark to validate the concept. The presently available parameters for the FCC IR quadrupoles indicate that they would be less demanding mechanically.

### 3.1 Electro-Magnetic Model

The electromagnetic model was analysed in ROXIE [12] mainly to verify that the magnitude of the field gradient with the simplified iron yoke with non-linear bh-curve is in agreement with the QXF EM-model. The electromagnetic forces were then computed at the nominal and ultimate design

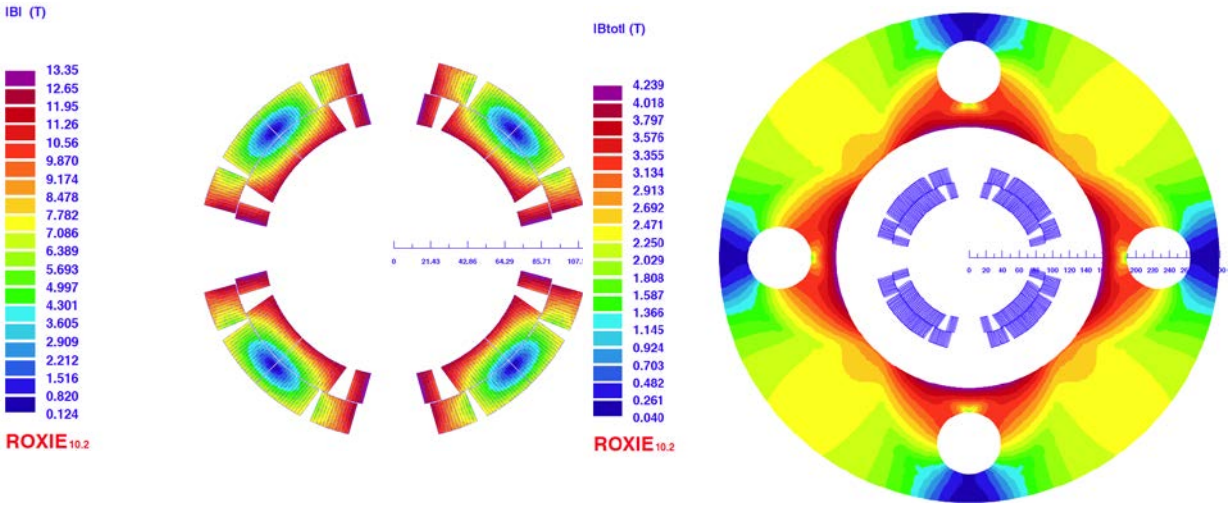


Figure 5 Electro-magnetic mode showing the field in the coils (left) and in the iron yoke (right).

gradients of 140 T/m and 155 T/m, respectively, and transferred to the structural model using the ANSYS2ROXIE-interface [13]. The field modulus in the coils and the simplified iron yoke at 155 T/m are shown in Figure 5. (For modelling reasons the model is rotated by 45 degrees hence representing a skew-quadrupole).

### 3.2 Structural analysis model

A fully parametric FE-model was created in ANSYS Classic using the APDL-programming language. Higher order PLANE183 structural elements were used for creating the mesh and all interfaces were modelled with CONTACT172 and TARGET169 elements. Friction coefficients and stick-slip behaviour were not included. The initial gap conditions simulating also the shimming were defined as input data for each interface separately.

**Table 1:** Material properties of main structural components

| Structural component | Material | Thermal contraction[a] (mm/m) | Elastic modulus (GPa) | |
|---|---|---|---|---|
| | | | Warm | Cold |
| Coil | $Nb_3Sn$ – epoxy-glass composite | Rad. 3.08<br>Azim. 3.36 | 52<br>44 | 52<br>44 |
| Wedge | Al-bronze | 3.12 | 110 | 120 |
| Collar | Nippon steel | 2.7 | 195 | 215 |
| Key | Stainless steel | 2.64 | 190 | 210 |
| Yoke | Iron | 2.02 | 210 | 225 |
| Outer Shell | Stainless steel | 2.9 | 195 | 215 |

[a] (300-1.9 K).

### *3.2.1 Material properties*

The elastic modulus and the integrated thermal contraction factor (293..1.9 K) of the materials are given in Table 1.

### *3.2.2 Coils and coil assembly*

The winding blocks of the coils were modelled with anisotropic material properties identical to those used in the QXF analysis including the Al-bronze wedges. The additional Al-bronze filler wedge was added on the outer layer and 0.2 mm thick epoxy-glass layer was modelled between the coil and the 2-mm-thick stainless steel loading plate. The polyimide layers of the ground insulation were not individually modelled, but a 1.875-mm-thick epoxy-glass layer was created on the outer surface of the coils. In addition, the collaring shoe (typically 0.5 mm stainless steel sheet) was not included in the coil-collar interface for this first conceptual study, but will be modelled in the more refined optimisation study.

The Ti-alloy pole wedges of the two types were connected to the coils through gap elements that also simulate the shims. The coil mid-plane interface was modelled in the same way with frictionless sliding contact. The stress relief notch in the pole wedges indicated in Figure 3 plays an important role in the stress distribution of the inner layer pole-turns and its dimensions were part of the optimisation process.

### *3.2.3 Collars and collar assembly*

The collar thickness was defined as 0.5 mm and all other parts as 1 mm. The collars were modelled as two over-lapping layers consisting each of a long and a short collar. A welded pin was used to connect the long collar to the short collar on the different layer. On the outer radius the short collar was made 0.5 mm smaller than the long collar. Therefore, the short collars could be considered essentially as filler except at the mating plane region, where they contribute to the lateral rigidity of the closed collar-pack.

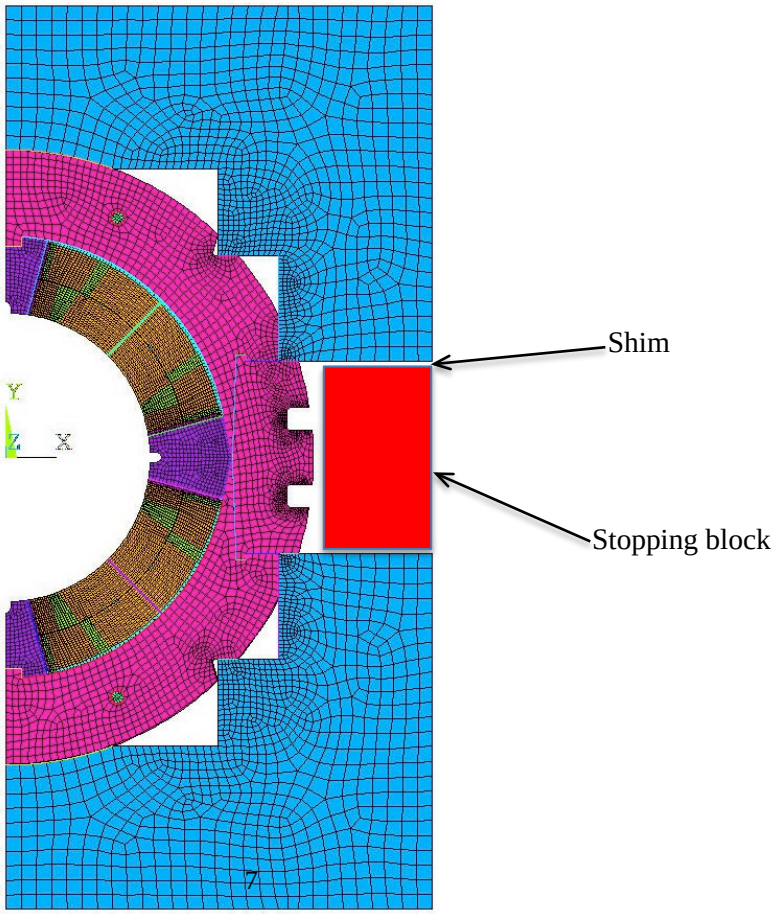


Figure 6 Collaring press contact tool and the optional stopping block.

The nose of the long collars locates in the slot of the pole wedge at the vertical plane and this interface can also serve for adjustment shim during the model magnet phase. On the horizontal plane the 12° taper of the long collar leg pushes the pole wedge inwards when the top and bottom collars are pushed together under the collaring press. This taper angle can provide the pole wedge with a 1.2 mm lateral travel. A shimming similar to the vertical plane could be realised by making the wedge in two parts and adding an adjustment shim in between them.

The collaring press contact tool shown in Figure 6 has five contact areas with each collar. The flexural stiffness of the collaring tool can be increased by adding an additional “stopping block” in the mid-plane and using a shim-based displacement control between the top and bottom halves. This also avoids accidental over-compression of the brittle Nb3Sn coils.

The first load-step was defined by applying a vertical displacement on the press-tool outer surface until the contact surfaces of the key-ways on the top and bottom collars were aligned to allow the insertion of the keys. The key section was chosen relatively large (10 x 12 mm) to limit the local stress around the key-ways.

The second load-step simulates the collared coil when the collaring press has been released and the load is taken by the collaring keys. The collared coil in this case deforms elliptically such that longer axis is along the vertical plane as shown in Figure 7.

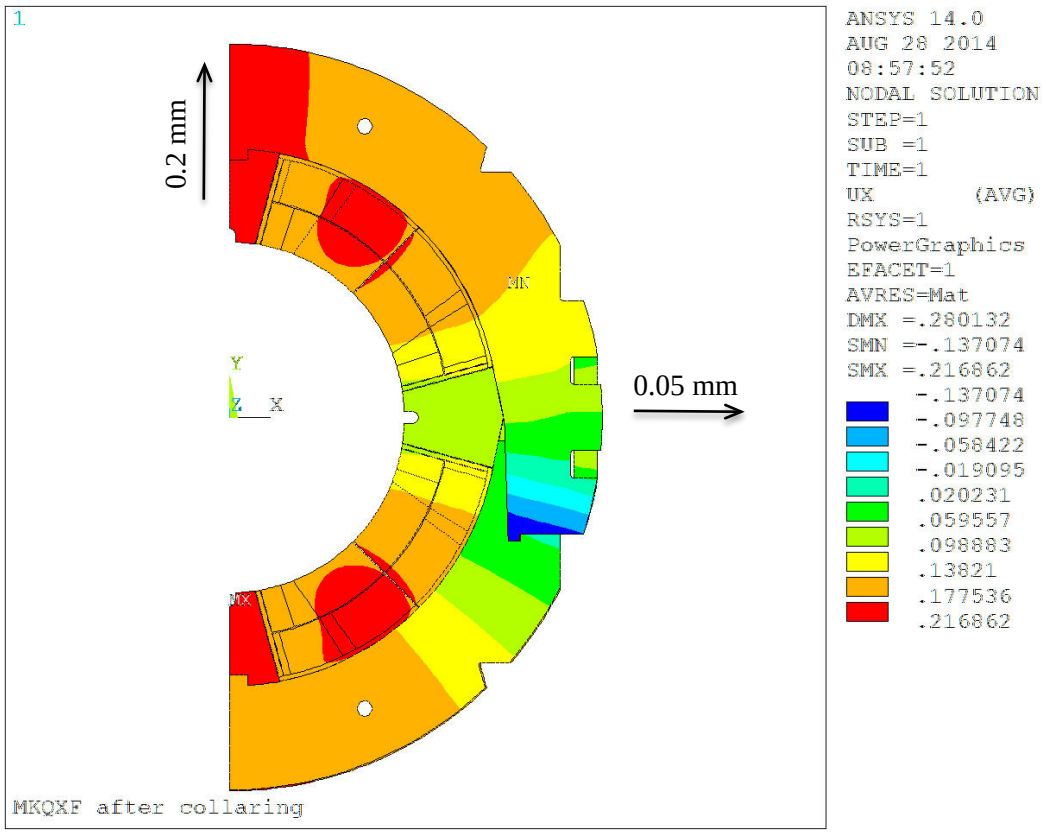


Figure 7 Radial displacement in mm after collaring.

### *3.2.4 Yoke and cold mass assembly*

The laminated yoke with an outer diameter of 600 mm is made of two halves and can have either a vertical or horizontal split. With the collared coil deformation described above, the horizontally split yoke the yoke inner radius does not enter in interference with the collared coil on the mid-plane and

the yoking press can be utilised to restore the circular geometry of the collared coil during the cold mass assembly.

The interface between the yoke and the collared coil was modelled with 0.4 mm nominal shim as shown in Figure 4 and frictionless sliding contact. In the undeformed state there is a line-to-line fit between the collars and the yoke when the yoke mid-plane is closed. With the enormous rigidity of the yoke laminations this guarantees the circular geometry of the collared coil and minimises the asymmetric deformation and distortion of the quadrupole symmetry.

The holes for the heat exchangers were modelled, but the cut-outs for the bus-bars were not included, as they only have a very minor impact on the mechanics of the cold mass. The yoke mid-plane was made tapered such that with the contact on the inner radius the outer radius has a 0.2 mm gap in the free state. This provides some elasticity to the yoke to store strain energy against the enormous Lorenz forces from the coils.

The optimal stress level and distribution in the coils was found when the yoke gap was left open by 0.18 mm on the inner radius at the ambient temperature. This, however, would be very difficult to control during the cold mass assembly in addition to guaranteeing the left-right symmetry. As only one or two heat-exchanger holes are used for cooling purposes the other two at the mid-plane can be used for controlling the gap. Increasing their diameter from 77 mm to 81.75 mm and placing a round aluminium bar or thick-walled cylinder in these locations provides a precise control of the yoke gap during the yoke assembly, that can be easily adjusted, if required. During the cool down the gap controller then shrinks away from the iron allowing the closure of the gap and hence ensuring the rigid envelope around the collared coil.

The 15-mm-thick stainless steel outer shell is welded at the mid-plane. The weld-shrinkage of 0.84 mm that is based on 11 T Dipole welding was modelled by applying a forced displacement on the mating faces of the half shells.

The third load-step in this structural analysis is after the completion of the cold mass assembly. The loading under the yoking press typically has only a small effect on the coil stresses, especially with the gap-controller, and it was not modelled for this analysis.

### 3.3 Load-steps

Six load-steps were considered in this analysis:

1. Under collaring press
2. After collaring
3. After cold mass assembly at 293 K
4. After cool down to 1.9 K
5. At 1.9 K and 140 T/m
6. At 1.9 K and 155 T/m

### 3.4 Design goals

In coil-dominated magnets the conductor positioning determines the field quality. Moreover, microscopic conductor movements can locally generate enough heat to drive the superconductor into the resistive state causing a quench. The coils shall, therefore, be clamped solidly to minimise any dimensional distortions and conductor movements. Too high compression, however, can cause irreversible degradation of the $Nb_3Sn$, again compromising the magnetic performance. The maximum value for the acceptable coil stress is still a subject of debate in the magnet community, but keeping it below 155 MPa at all times is generally considered safe.

At the pole regions the Lorenz forces are unloading the coil from the poles. In the case of the integrated pole, where the turns are glued to the pole, a tensile stress of the order of 10-20 MPa may break this bond or cause cracks in the resin, which may degrade the performance. With the pole-loading concept, however, this degradation is not present, as the pole is not bonded to the coils. In this sense the pole-loading is expected to behave similarly to the Nb-Ti magnets of the LHC short model program, where unloading at the poles did not have any noticeable effect on the quench performance.

The main source of the coil pre-stress is the collaring process. This process can be well controlled and the shimming is determined based on the coil dimensional inspection using CMM. The collared coil deformation and consequent bending stresses and distortions from the quadrupole symmetry are minimised using very rigid collars made out of high manganese steel. The collar inner and outer radius is 115 mm and 160 mm, respectively.

The yoke assembly provides the collared coils a static and very rigid mechanical envelope. It is important to rely on structural references and avoid floating structure. This is achieved by using the gap-controllers at the ambient temperature and firmly closing the yoke gap at the operating temperature. The yoke gap shall also remain firmly closed up to the highest design current. The stainless steel outer shell tension at the ambient temperature shall remain below 230 MPa.

## 3.5 Results

### *3.5.1 Coil stress*

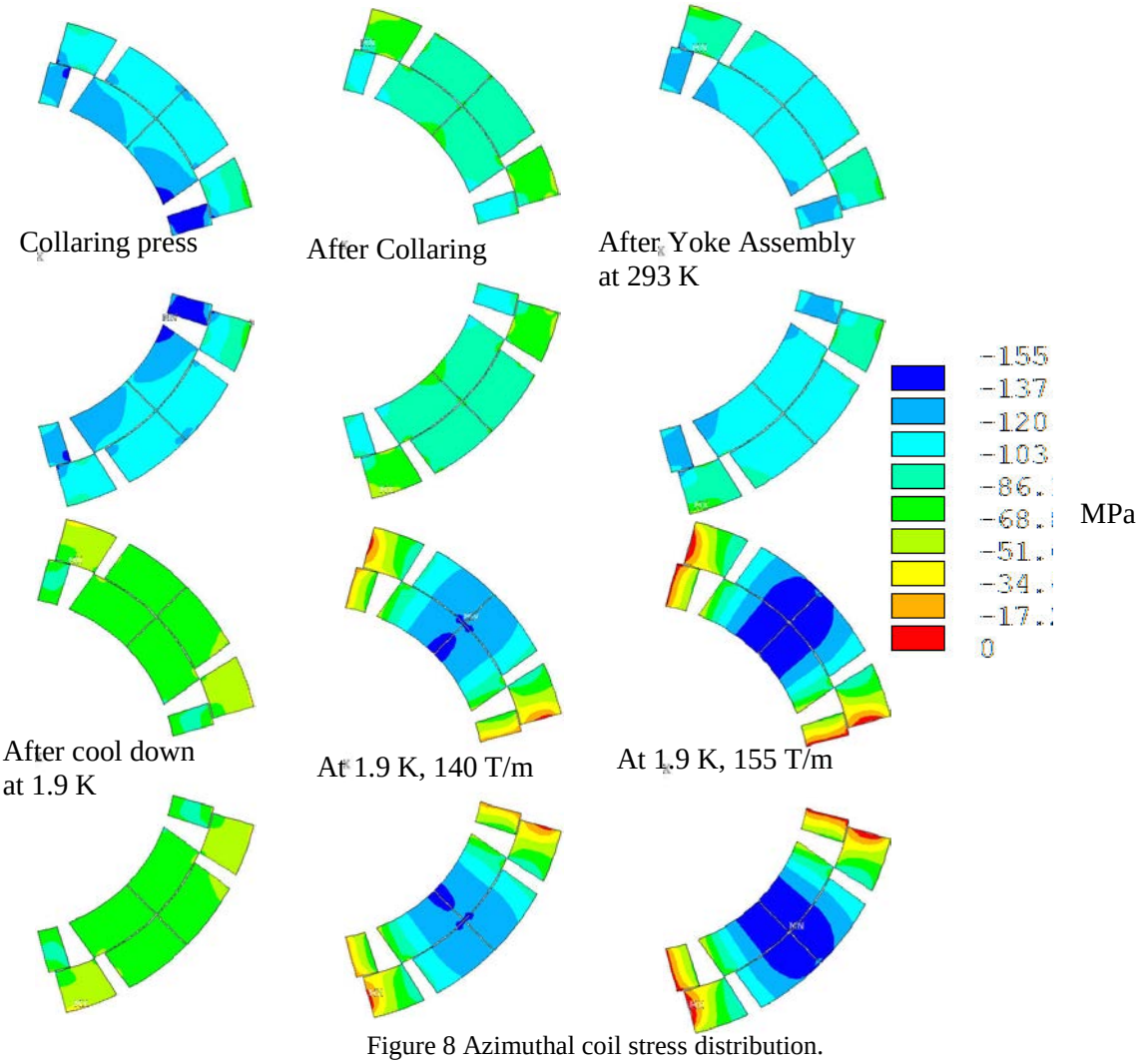


Figure 8 Azimuthal coil stress distribution.

The Figures 8 and 9 illustrate the azimuthal coils stress evolution for the six load steps. The maximum value of about -153 MPa is reached in the inner layer pole-turn near the mid-plane under the collaring press. After releasing the press the spring back and stress re-distribution reduces the coil stress by about 45 MPa the mean stress being -85 and -70 MPa in the inner and outer layer, respectively. The yoke assembly restores most of the elliptic deformation of the collared coil and increases the coil compression by about 40 MPa bringing the maximum stress to -133 MPa. As the yoke gap is slightly open (0.18 mm) at the ambient temperature, there is still a slight asymmetry in the stress distribution of the coils indicating distortion from the quadrupole symmetry.

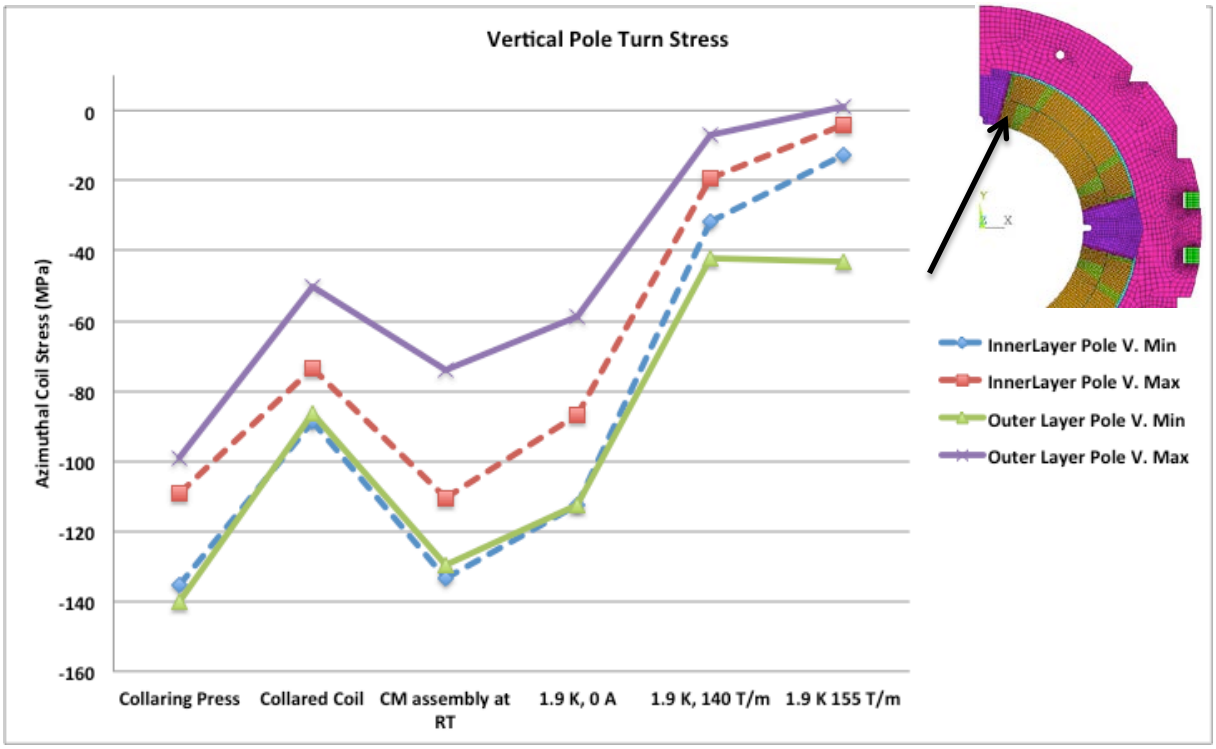


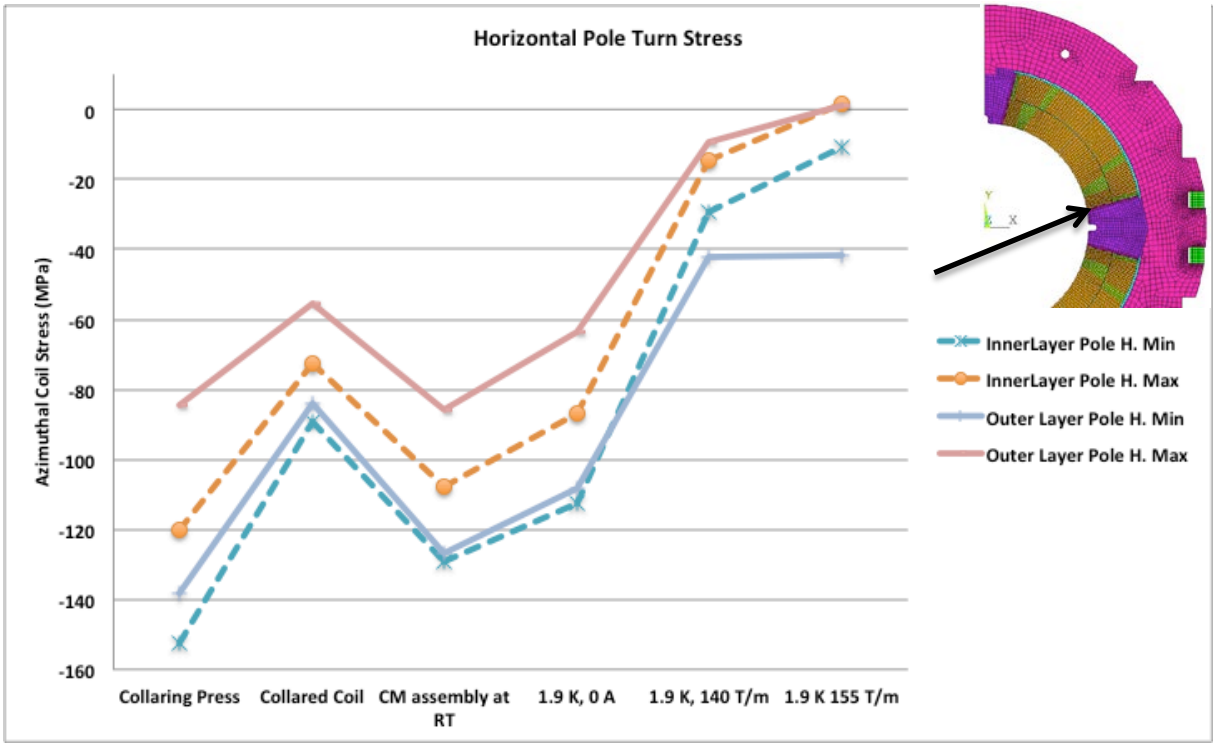

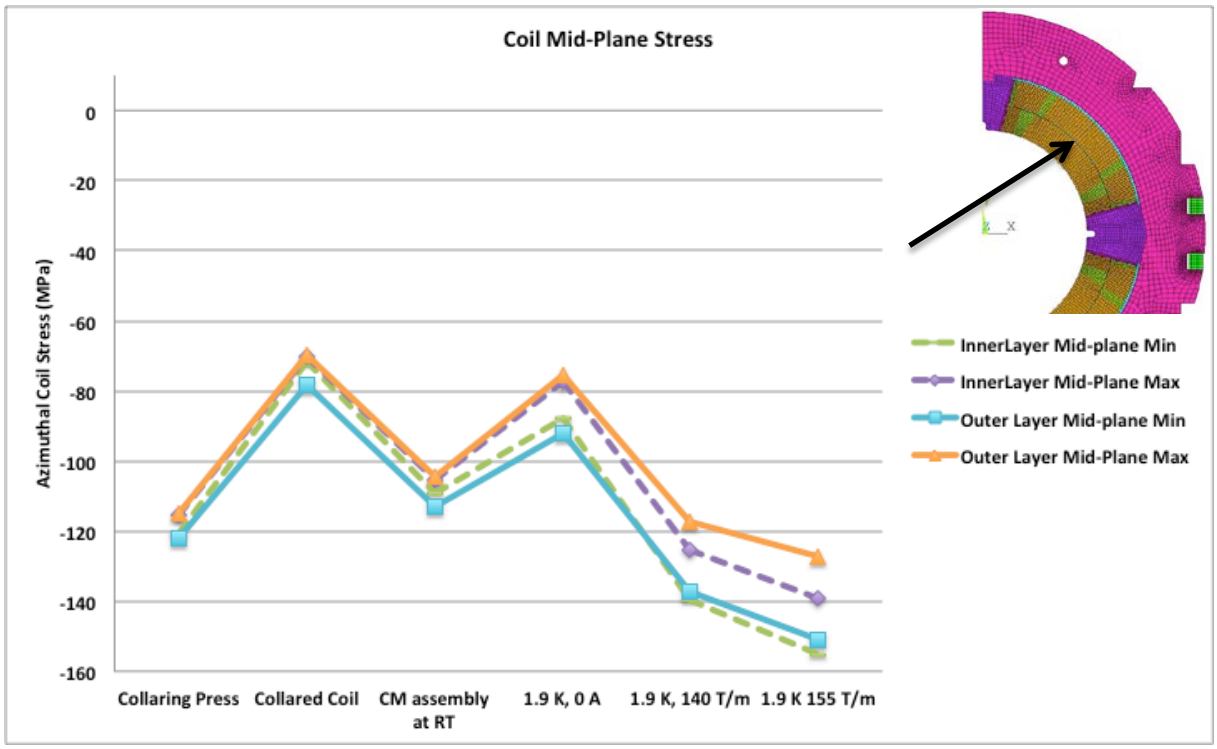


Figure 9 Azimuthal coi stress evolution in MPa.

During the cool down to 1.9 K, the collared coil contracts more than the iron and the coil pre-compression is reduced by about 20 MPa. With the yoke gap firmly closed the stress distribution is now perfectly symmetric and the poles have highest and the mid-plane the lowest pressure to counter-balance the effect of the Lorenz forces.

At 140 T/m and 155 T/m the very rigid structure keeps the coil stress distribution very uniform across the coils without exceeding the safe stress levels. At 155 T/m the pole pressure is practically zero, but as stated above, this is not expected to have any deleterious effects on the coils or the performance. At the coil mid-plane the maximum stress on the inner layer ranges from -140 MPa at 140 T/m to -155 MPa at 155 T/m.

Similar graphs for the QXF magnet based on bladder-and-key structure can be found in Appendix A. It can be seen that after cool down there is relatively large gradient in the pole turns as well as on the outer layer mid-plane during powering. As the coils are identical in both FE-models, the radial displacement of the node on the outer radius at coil mid-plane can compared between the collared and bladder-and key structures. During the cool down this nodes moves in by 432 µm (194 µm) in bladder-and-key structure (collared structure). The electro-magnetic forces at 155 T/m push this node outwards by 56 µm (39 µm) indicating higher structural rigidity of the collared structure.

### *3.5.2 Collar stress*

The equivalent stress (Von Mises) distribution in the collars is shown in Figure 10. The areas with stress over 300 MPa are indicated in grey colour and these are the areas around the key-ways that typically plastify during the assembly process.

### *3.5.3 Yoke and Gap-controller*

Figure 11 shows the behaviour of the yoke and the gap-controller after the yoke assembly, after cool down to 1.9 K, and with 155 T/m gradient. The red arrows on the yoke inner diameter indicate the reaction forces with the collared coils and on the outer radius with the outer shell. The relative

magnitude of the reaction is given by the arrow length. At the yoke mid-plane the red arrows show the reaction between the half-yokes and the contact with the gap-controller. At 293 K the gap is open controlled by the Al-bar. After cool down the gap is firmly closed and remains closed up to 155 T/m.

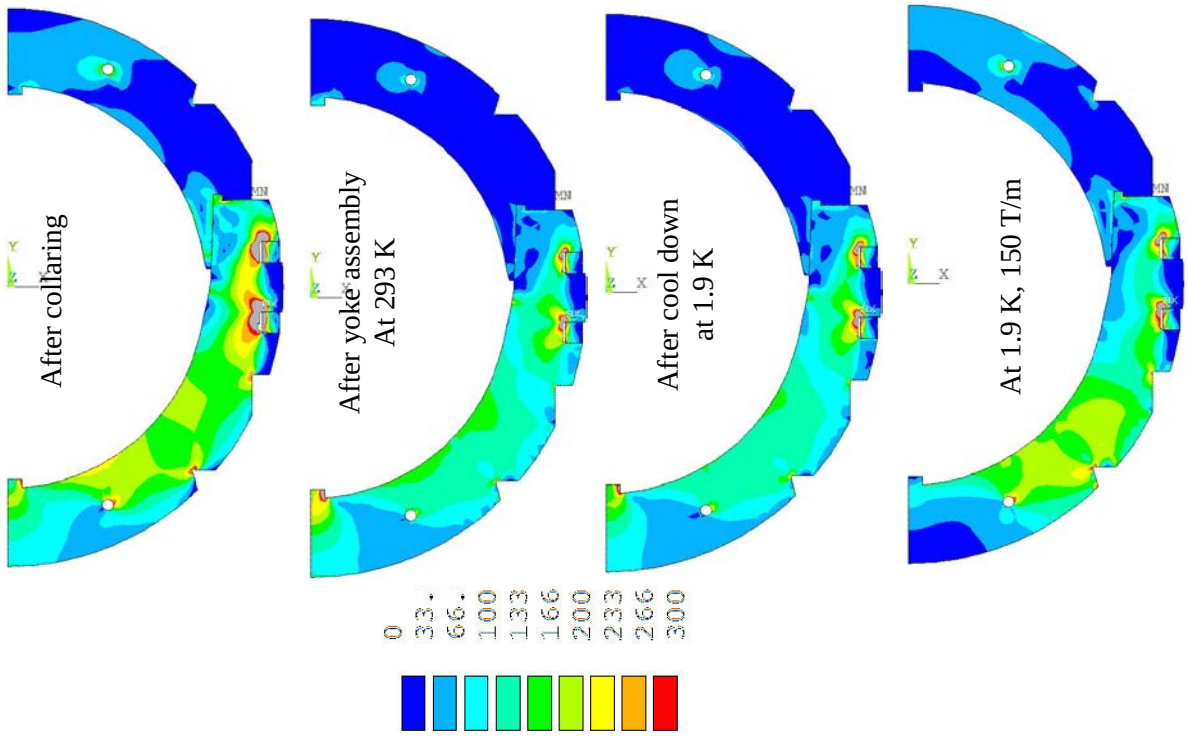


Figure 10 Equivalent collar stress in MPa.

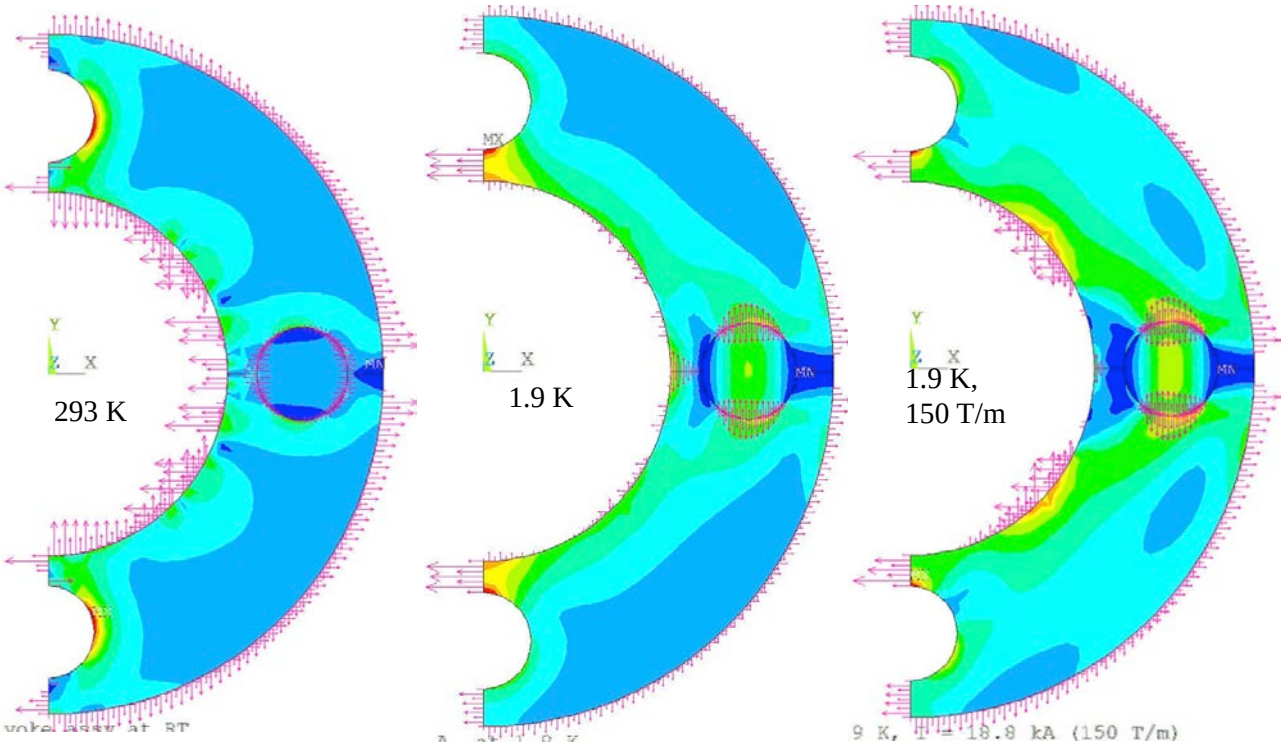


Figure 11 Yoke and gap-controller bahavior. The reaction forces with the collared coil and the shell are indicated with red arrows.

### 3.6 Next steps

Before entering in the final manufacturing design phase of a demonstrator magnet a more refined optimisation should be carried out. For example a more detailed model of the ground insulation and the collaring shoe should be included enabling the collar stress distribution to be further optimised. A sensitivity analysis shall be carried out with realistic tolerances for the dimensional variation of the coils along with the manufacturing tolerances of the components. The impact of the deformed coil shape on the field quality can easily be computed including all these variations.

## 4 Conclusions

A new mechanical design concept for a Nb3Sn quadrupole suitable for industrial production has been developed. It relies on well-proven construction methods used for LHC main magnets. The FEA shows that the coils can be solidly clamped whilst staying well within the generally accepted range of stress in the brittle Nb3Sn coils.

The coil pre-stress is applied in a well-controlled manner during the collaring and easily tuneable shimming allows the compensation of coil dimensional variations and mechanical tolerances of the magnet components. To counteract the very large electro-magnetic forces the pole-loading concept provides the “tuning knobs” to tailor the coil pre-stress such that it is the highest at the pole and the lowest at the coil mid-plane. The tapered-shape of the mid-plane poles together with the dipole-type collars makes it possible to carry out the collaring process in a dipole-type press and simultaneously over the entire coil length. The very rigid collars minimise the elliptic deformation after the collaring.

The horizontally split iron yoke with a closed gap at operating temperature provide an almost infinitely rigid structure around the coils minimising any conductor movements and distortions from the ideal coil geometry. The stainless steel shell assembly parameters are achievable and the stresses remain at an acceptable level at all times.

A short demonstrator magnet could be constructed and tested with a very moderate investment in magnet components using the existing QXF coil geometry. The main advantage would be that all existing coil fabrication tooling could be used as such profiting from the QXF conductor and coil development.

The collared quadrupole concept can easily be extended to any length, and also applied on a 2-in-1 configuration, which opens very interesting prospects for the FCC main quadrupoles.

## 5 References

[1] M. Karppinen et al., “Design of 11 T Twin-Aperture Nb3Sn Dipole Demonstrator Magnet for LHC Upgrades”, IEEE Trans. Appl. Supercond., vol. 22, no. 3, Jun. 2012, Art. No. 4901504.

[2] L. Bottura, “The FCC Magnet Program: Challenges and Opportunities for HTS“, http://indico.cern.ch/event/308828.

[3] S. A. Gourlay et al., “Magnet R&D for the US LHC Accelerator Research Program (LARP)”, IEEE Trans. on Appl. Supercond., v.16, Issue 2, June 2006, p. 324.

[4] A.V. Zlobin, “Status of Nb3Sn Accelerator Magnet R&D at Fermilab”, EuCARD - HE-LHC'10 AccNet mini-workshop on a “High-Energy LHC”, 14-16 October 2010, FERMILAB-PUB-11-001-TD, January 2011. CERN Yellow Report CERN-2011-003, pp. 50-58.

[5] R. C. Bossert, et al., “Development and Test of LARP Technological Quadrupole Models of TQC Series,” IEEE Trans.on Appl. Supercond., v. 18, Issue 2, June 2008, p. 175.

[6] S. Caspi et al., “The use of pressurized bladders for stress control of superconducting magnets,” IEEE Trans. Appl. Supercond., vol. 11, 2001.

[7] P- Ferracin et al., “Magnet Design of the 150 mm Aperture Low-β Quadrupoles for the High Luminosity LHC”, IEEE Trans. on Appl. Supercond., vol. 24, no. 3, June 2014.

[8] F. Savary et al., “Design, assembly and test of MBHSM101, a 2-m long practice model made of a single coil wound with Nb3Sn cable at CERN”, ASC-14, Charlotte, August 2014.

[9] G. Spigo et al., “Design and Performance of a New 50 mm Quadrupole Magnet for the SSC”, Supercollider 5, Plenum Press, New York, 1994 p. 647.

[10] G. Chlachidze et al., “Quench Performance and Field Quality of 90-mm Nb3Sn Quadrupoles of TQC Series”, Proceedings of IPAC2012, New Orleans, Louisiana, USA, p.3581.

[11] M. Juncho, “Support Structure Design of the Nb3Sn Quadrupole for the High Luminosity LHC”, ASC-14, Charlotte, August 2014.

[12] ROXIE code for an electromagnetic simulation and optimization of accelerator magnets, http://cern.ch/roxie.

[13] A. Milanese, “A method to transfer concentrated Lorentz forces to a finite element mechanical model”, CERN TE-Note-2010-006 (EDMS NO. 1092691).

## Appendix A: QXF (bladder-and–key) coil stress evolution

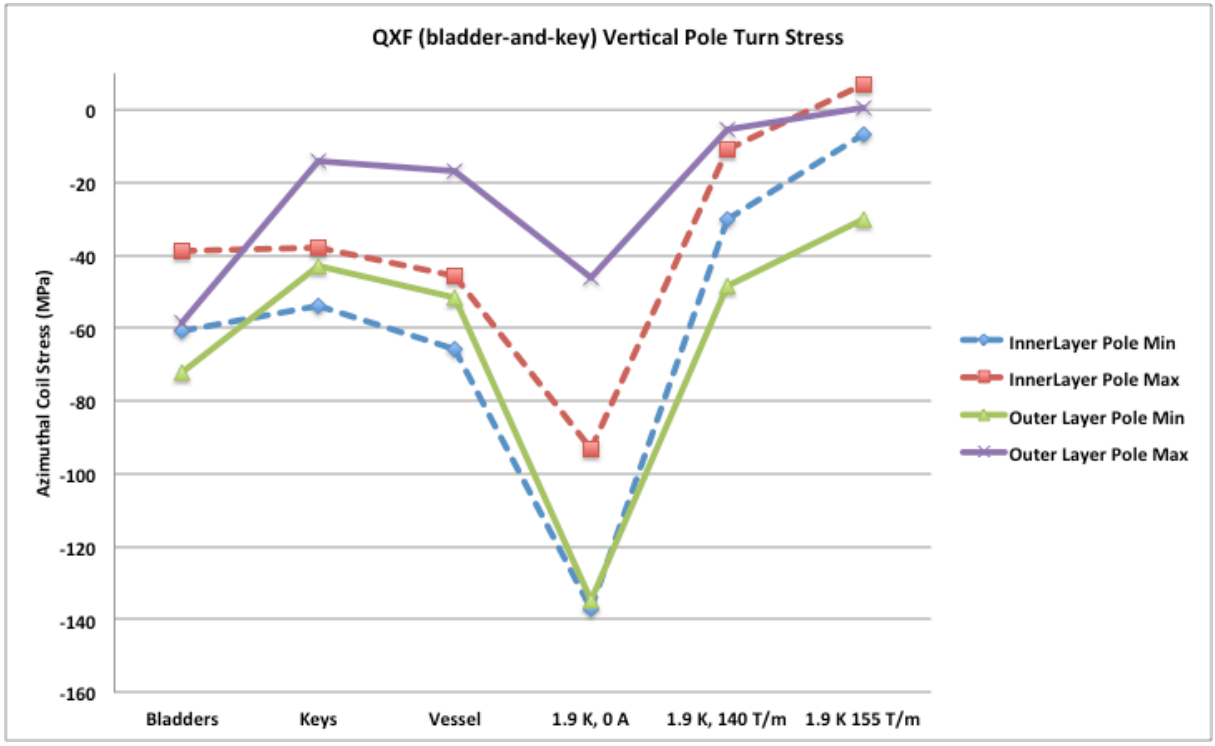


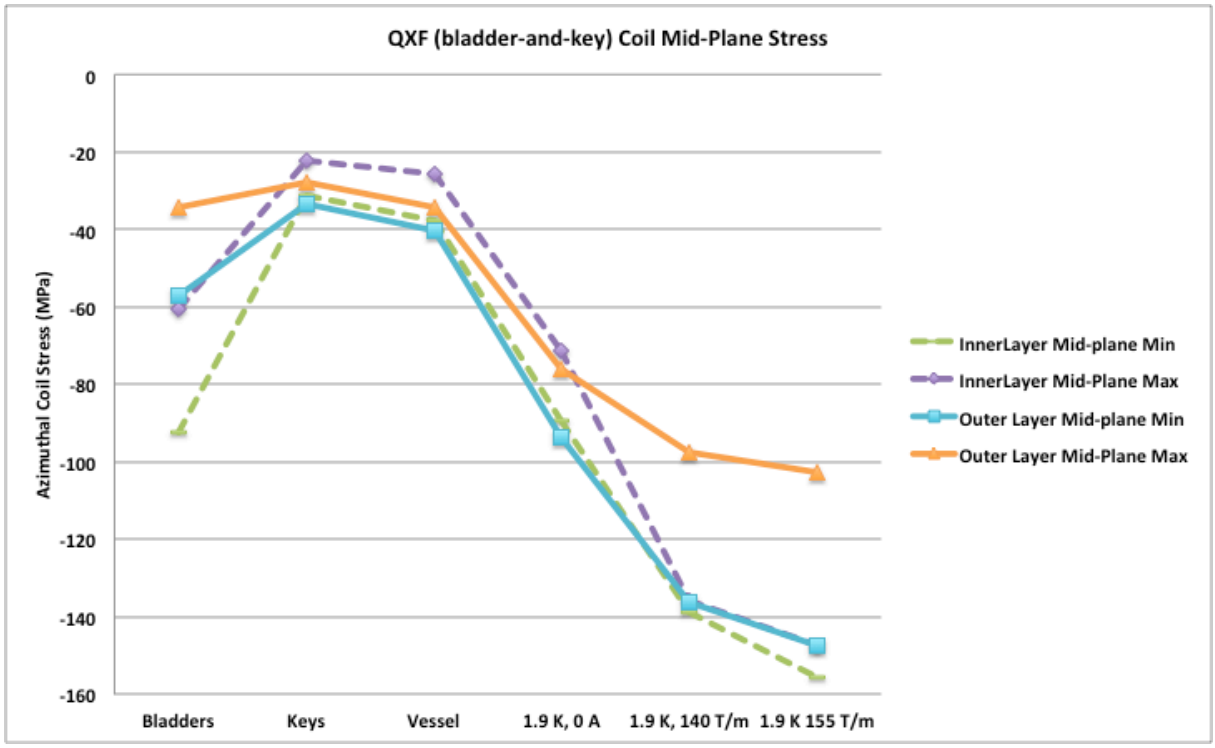


Figure 12 Azimuthal pole-turn and mid-plane turn stress evolution in QXF coils in the bladder-and-key structure.